DOI: 10.1002/ admi.201700722
Article type: Full Paper

Title: Decreasing Defect-state Density of $Al_2O_3/Ga_xIn_{1-x}As$ Device Interfaces with InO_x Structures

Jaakko Mäkelä, Marjukka Tuominen, Johnny Dahl, Sari Granroth, Muhammad Yasir, Juha-Pekka Lehtiö, Rami-Roope Uusitalo, Mikhail Kuzmin, Marko Punkkinen, Pekka Laukkanen*, Kalevi Kokko, Roberto Félix, Mika Lastusaari, Ville Polojärvi, Jari Lyytikäinen, Antti Tukiainen, Mircea Guina*

J. Mäkelä, M. Tuominen, Dr. J. Dahl, Dr. S. Granroth, Dr. M. Yasir, J.-P. Lehtiö, R.-R. Uusitalo, Dr. M. Kuzmin, Dr. M. P. J. Punkkinen, Dr. P. Laukkanen, Prof. K. Kokko
Department of Physics and Astronomy, University of Turku, FI-20014 Turku, Finland
E-mail: jaakko.m.makela@utu.fi, pekka.laukkanen@utu.fi

Dr. M. Kuzmin
Ioffe Physical-Technical Institute, Russian Academy of Sciences, St. Petersburg 194021, Russian Federation

Dr. R. Félix
Renewable Energy, Helmholtz-Zentrum Berlin für Materialien und Energie GmbH, Hahn–Meitner-Platz 1, D-14109 Berlin, Germany

Dr. M. Lastusaari
Department of Chemistry, University of Turku, FI-20014 Turku, Finland

Dr. V. Polojärvi, Dr. J Lyytikäinen, Dr. A. Tukiainen, Prof. M. Guina
Optoelectronics Research Centre, Tampere University of Technology, FI-33101 Tampere, Finland

Keywords: GaAs, oxide, interface, defects, HAXPES

Control of defect densities at insulator/$Ga_xIn_{1-x}As$ interfaces is essential for optimal operation of various devices like transistors and infrared detectors to suppress for example non-radiative recombination, Fermi-level pinning, and leakage currents. We report that a thin InO_x interface layer is useful to limit the formation of these defects by showing effect of InO_x on quantum efficiency of $Ga_{0.45}In_{0.55}As$ detector and on photoluminescence of GaAs. A study of the Al_2O_3/GaAs interface via hard x-ray synchrotron photoelectron spectroscopy reveals chemical structure changes at the interface induced by this beneficial InO_x incorporation: the InO_x sheet acts as an O diffusion barrier that prevents oxidation of GaAs and concomitant As bond rupture.

1. Introduction

An oxide/$Ga_xIn_{1-x}As$ interface is frequently found as part of various device components (e.g., metal-oxide-semiconductor high electron mobility transistor, MOS-HEMT, structure and IR detectors)[1-8] currently used in electronics and in the design of many a potential future device (e.g., III-V MOS field-effect transistor, MOSFET, and tunnel field-effect transistor, TFET).[9-12] However, oxide/$Ga_xIn_{1-x}As$ interfaces are usually considered as non-optimized, adversely affecting the device performance: namely, they contain a high density of material defects that cause electronic defect states in the band-gap area (gap-states), which further increase the leakage current, non-radiative recombination, and Fermi-level pinning for example. With the continuous development of wireless communication and intelligent transport systems, developing ways to control/reduce defect states concentrations in oxide/$Ga_xIn_{1-x}As$ interfaces becomes an essential task in order to improve the performance of devices based on III-V semiconductors.

Indeed, the nature of these interface defects as well as the methods to control their formation have been the subject of a vast body of investigations [e.g., Refs. 13-23]. In previous studies, these defect states have been found to arise, amongst others, from group-V dimers; group-V and group-III dangling bonds; and III-Ox or V-Ox phases. Thus, the identification of defect origin(s) is an open issue. There appears to be a consensus that the high oxidation state of Ga (i.e., Ga_2O_3 type) increases defect density and is more harmful than the corresponding oxides of In.[20-23] However, the mechanism responsible for Ga_2O_3-related gap states in $Ga_xIn_{1-x}As$ remains unclear. Methods to decrease the defect concentrations at an oxide/$Ga_xIn_{1-x}As$ interface should be further developed to match the famous industrial workhorse of SiO_2/Si in applications where interface defects limit the performance. A potential approach, presented

recently,[19,23] includes the deposition of a thin In layer on GaAs, followed by the oxidation of such In-terminated GaAs before the growth of an insulator film. This method leads to a crystalline oxidized In-containing GaAs surface: GaAs(100)$c(4\times2)$-InO_x, which is promising to be incorporated into device structures, because it is found to increase photoluminescence (PL) intensity of GaAs, ascribed to result from a reduction in defect state density.[23]

Here we demonstrate the incorporation of this InO_x interface layer into an optoelectronic device structure, namely $Ga_xIn_{1-x}As$ infrared detector. We show how the InO_x layer can be included in the detector process so that the external quantum efficiency (EQE) increases due to InO_x. Furthermore, we have investigated the chemical structure of the Al_2O_3/$Ga_xIn_{1-x}As$ interface via hard x-ray photoelectron spectroscopy (HAXPES), in connection to the PL intensity comparison, to elucidate Ga-O-mediated defect-state formation. High resolution HAXPES As 3d spectra reveal a relation in the intensity of a spectral feature associated with As dangling bonds to the concentration of defect gap states. A defect-formation path which is consistent with recent calculations[24] is suggested.

2. IR detectors with InO_x interface

The layer structure and a cross-sectional view of a processed IR detector device is depicted in **Figure 1**. A thin p^+-$Ga_{0.75}In_{0.25}As$ serves as a pseudomorphic window layer to diminish the diffusion of minority charge carriers to the surface. A similar structure has been shown[25] to have high small-signal compression current along with high optical responsivity. After MBE growth, a protective 50 nm As cap layer was deposited on the topmost surface. The cap was removed in a separate vacuum system by heating the sample to ca. 400 °C for 15 min before indium deposition and crystalline oxide surface preparation, similar to one used for GaAs(100)[19] (described below), and atomic layer deposition (ALD) of Al_2O_3.

A standard optical lithography procedure was used to process the sample pieces into IR detector devices. Initially, four 3×2.15 mm^2 mesas were dry etched with a commercial inductively coupled plasma reactive ion etching (ICP-RIE) dry etch system with a Cl_2/N_2 plasma on the samples. Large area samples were produced in order to minimize effects from the sidewalls, to more reliably characterize the surface related performance. On the mesa areas, grid openings to Al_2O_3 film were etched with (1:10) $NH_4OH:H_2O$. Top-side 50/50/200 nm Ti/Pt/Au grid metal with a lift-off procedure was deposited, resulting in a total area of 1.84 mm^2 on a single mesa. Following the top lift-off metallization, bottom-side 5/5/30/90 nm Ni/Au/Ge/Au sheet metal was deposited and thermally annealed at 370 °C for 60 s to form an optimal Ohmic contact.

The EQE from two IR detector mesas, which fitted the experimental EQE setup, from each sample were measured to characterize the wavelength dependence on the performance of the devices. White light was projected through a monochromator and lenses to produce a spot of 100×100 μm^2 using a 27 Hz frequency chopper with a feedback to filter out the response caused by ambient light. The resulting responsivity has a very low noise due to long duration of illumination. The light source is calibrated to maintain constant intensity with a photodiode feedback, for reproducible measurements. Wavelength range of 1120 - 1800 nm was swept and the response of each point was measured. Calibration was done by initially measuring the response from a Ge diode, the responsivity of which was known and the data was scaled accordingly.

Responsivities observed for the crystalline oxide detectors (four devices characterized in total) and reference devices (two devices characterized in total) are plotted in **Figure 2**. The responsivity of the devices, excluding one clearly off from the trend, is in the range of 0.4 - 0.5 AW^{-1} in the 1200 - 1600 nm wavelength range. A peak responsivity value for the

crystalline oxidized GaInAs photodetector was 0.52 AW^{-1} and for the reference sample 0.46 AW^{-1}. The peak EQE values in this range are 0.49 and 0.42, respectively. A notable difference is the increasingly higher responsivity of the crystalline oxide samples towards lower wavelengths, which are absorbed closer to the surface, another proof for higher surface quality due to a lower degree of non-radiative recombination. This is well illustrated also by the higher rise of the low wavelength responsivity with a higher In-content that corresponds closer the $c(4\times2)$ surface as compared to lower In-content closer to (1×1) discussed in section 3. These results along with the improved responsivity overall clearly indicate the benefit of passivation via crystalline oxide InO_x-interlayer.

3. Interface analysis

3.1. Sample preparation

To investigate the origin of the beneficial effect of the crystalline oxide layer, four GaAs(100) samples were prepared in an in-situ ultrahigh vacuum atomic layer deposition (UHV-ALD) system. 5×10 mm^2 sample pieces were cut from an epi-ready 2.5×10^{18} cm^{-3} Si-doped n-GaAs wafer. Samples were cleaned using Ar^+-sputtering (at 1×10^{-7} mbar Ar pressure, 10 mA emission current, 1 kV acceleration voltage and 350-400 °C sample temperature) and post-annealing cycles at 400-450 °C until a prominent (6×6) low energy electron diffraction (LEED) pattern was observed. This reconstruction is characteristic for a fairly Ga-rich surface[26] and could reliably be reproduced to achieve atomically smooth surface. On three of the samples, different amounts of In, estimated to be in the range of 0.2 - 2 monolayers, were deposited, annealed until a $c(8\times2)$ was observed, then simultaneously oxidized and annealed in UHV in a way that produced a crystalline oxide terminated GaAs(100)-InO_x surface, the detailed procedure of which is described elsewhere.[19] One reference sample with no indium or oxidation was also included in the following tests. The final reconstruction is observed to depend on the amount of In deposited with highest tested amount of In exhibiting (4×3) and slightly lower $c(4\times2)$. With the lowest tested amount of In, only a (1×1) LEED pattern is

detected, which could be interpreted as a thin amorphous oxide that only slightly attenuates LEED signal from sub-surface layers and possibly only small areas of crystalline surface. However, surprisingly sharp and prominent LEED spots seen in the second inset of **Figure 3** imply an un-reconstructed bulk-like terminated surface. It is worth noting that a LEED coherence length is short (about 10 - 20 nm), and therefore, the presence of local amorphous defect areas cannot be excluded because of a sharp LEED pattern, while possible amorphous areas are expected to broaden the oxide related XPS emission components. Subsequently, the samples were transferred in-situ to the ALD chamber and a 12 nm Al_2O_3 film was deposited. H_2O and trimethylaluminum (TMA) were used as precursor gases. The sample temperature was kept at 180 °C during deposition.

3.2. PL analysis

The samples, interfacial areas of which were protected by the Al_2O_3 film, could be measured with an ex-situ PL system to qualitatively characterize the density of defect states. Figure 3 shows the PL spectra for each of the samples along with the LEED figures of the starting surface of GaAs(100)(6×6) and the observed intense (1×1)-InO_x as insets. For LEED patterns of the other surfaces, we refer to our previous works.[19,23] The least amount of non-radiative recombination is observed for the *c*(4×2) sample, and the most for the (1×1) sample. The PL results indicate that there is an optimal amount of In which corresponds to an essentially much more passivated interface.

3.3. HAXPES study and analysis

To investigate the passivation mechanism, HAXPES measurements of the As 3d and In 3d core levels were carried out at the High Kinetic Energy Photoelectron Spectrometer (HIKE) endstation located at the BESSY II KMC-1 beamline at Helmholtz-Zentrum Berlin (HZB).[27,28] The samples were probed as-is, for the main goal was to probe the effects caused by the different interfaces at Al_2O_3/GaAs. Photon energies, *hv*, of 2020 eV - 7332 eV were used to probe the interface by varying the information depth of the measurements, i.e. largely

differing inelastic mean free paths (IMFPs) or attenuation lengths, in the measured signal. **Figure 4** shows comparison of the As 3d spectra from Al_2O_3/GaAs(100)(6×6), *c*(4×2)-InO_x and (4×3)-InO_x measured at $h\nu$ = 4020 eV. The data in Figure 4 is calibrated to the same binding energy (BE) at peak maximum, normalized to equivalent maximum intensity and similar background level on the BE side. There are some distinct and consistent features separating the spectra. The (6×6) sample has increased emission features (marked by arrows in Figure 4) at both the low and high BE sides of the bulk component, as compared to the InO_x samples. Although all the As 3d spectra are relatively narrow, these marked broadenings for the (6x6) sample are clearly distinguished from the noise level. These features are utilized along with surface sensitivity and other peak boundary conditions in the peak fitting procedure discussed next. **Figure 5** a) shows the HAXPES As 3d spectra using different excitation energies (i.e., varying information depths) on Al_2O_3/GaAs(100)(6×6); spectra were normalized to their maximum intensity. In Figure 5 b), normalized intensities from the samples with an InO_x interlayer ($h\nu$ = 4020 eV) along with the In $3d_{5/2}$ with similar intensity calibration as insets are shown.

Fitting of peaks arising from different chemical states or energy levels was done using CasaXPS software version 2.3.16.[29] Here, we focus on the curve fit analysis results of the high resolution As 3d peaks, since effects on Ga bonding have previously been investigated in detail.[20-23] In our study, Ga 3d, that is commonly used for high resolution characterization of Ga chemical states[23,30] could not be utilized due to highly intense tail from adjacent O 2s peak. However, for similar InO_x interface and thin Al_2O_3, reduced oxidation of Ga has been observed.[23] Calibration of the BE scale for each excitation energy was carried out by adjusting the BE of Au $4f_{7/2}$ peak to 84.0 eV, measured from a clean gold foil that was in electrical contact with the sample. For the curve fit analysis of the As 3d spectra, offset Shirley background was subtracted. Voigt profile approximation of Gaussian-Lorentzian

product [GL(50)] peak profile was used that had a doublet separation of 0.71 eV and a spin-orbit splitting (SOS) ratio between the $3d_{3/2}$ and $3d_{5/2}$ of 0.67. Five different peak pairs in total were needed to obtain a suitable fit for the As 3d spectra of the sample series. Bulk peak BE position was fixed to an interval of 41.3 - 41.57 eV and all of the peak widths to 0.50 - 0.63 eV and the maximum FWHM variance for a given peak at a given $h\nu$ to ±0.05 eV. Two of the peaks were identified at a higher BE from bulk, one at +0.25 eV and one seen only for the Al_2O_3/GaAs(100)(6×6) sample with $h\nu$ = 2020 eV at +1.0 eV. Two components were observed at lower BE, -0.65 eV and -0.40 eV.

The -0.65 eV component was seen for most of the peaks on a broad range of IMFPs as well as the high intensity +0.25 eV component. The components at -0.40 eV are assigned straightforwardly to As-In bonding as they correspond well with the amount of In at each interface also roughly confirmed by the relative intensity of In 4d and In 3d peaks. InAs chemical states lie at a lower absolute BE than GaAs consistent with the separation of -0.4 eV.[31] By further comparing the intensities of PL, i.e., relative defect state densities, it is observed that for samples that have higher PL also tend to have lower intensity of -0.65 eV peak. This observation suggests that this peak consistently characterizes the bonding environment of defects.

The +1.0 eV separation in GaAs is characteristic for sub-oxides[22,32] and in the case of GaAs, different kinds of sub-oxide environments are possible. These states are presumed to be located at the interface, which is supported by the fact that a small +1.0 eV peak is observed only for the non-InO_x containing sample with lowest $h\nu$, i.e., with highest interface selectivity. Only a minor As-O contribution is to be expected due to the Ga-rich starting surface. This assumption is supported by many studies which assign midgap defect states to As-bonds that have an amphoteric nature, caused by vacancy-antisite and/or dimer-like positioning of As

that can correspond to local deficiency in Ga-bonds.[24,33-25] Group III oxides are typically more stable than group V oxides, and preferential bonding of O to Ga is commonly observed in III-V compounds.[14,36-38] The highest -0.65 eV component intensity for the Al_2O_3/GaAs(100)(6×6) observed with the oxide peak is consistent with the appearance of As dangling bonds induced by the Ga-O bond formation. Because for this sample there is a high presence of oxygen, oxidation of As also takes place. Indeed, a negative shift due to charge accumulation is to be expected in n-type GaAs for defective states in As-bonding due to their amphoteric[24] nature. An interesting observation made here is that this As dangling bond related component originates from a broad range of depths according to the spectroscopic results.

A surprisingly intense component necessary for fitting an envelope that reproduces the spectra is required at a low BE difference of +0.25 eV. There is some correspondence between the appearance of As dangling bond peak and this interface related component. Again, this peak pair shows high relative intensities in As 3d spectra that was measured with a broad excitation energy range, and especially for the Al_2O_3/GaAs(100)(6×6). In contrast for the Al_2O_3/GaAs(100)-InO_x this component is smaller and decays faster. Considering the observations above, we assign this peak to band bending, i.e., charge redistribution effects, which have been observed with HAXPES for GaAs(100).[39] This is a natural consequence of charge accumulation at the interface, causing upward bending in the range of tens of nanometers for GaAs. A potential affecting the energy levels in the range of CBM to midgap in the vicinity of the interface can easily affect the position and width of the envelope peak in the range of 0.1 - 0.2 eV. [39] It is to be noted that fitting two similar peaks (bulk 'flat band' and interface 'bent band') to take this effect into account is a rough approximation but accurate enough, especially in a non-quantitative estimation. A fitting algorithm for reproducing a single bulk peak with bent bands at the interface region is a complicated task because, as is

shown above, the defect states are not located abruptly at the interface but also at the subsurface region. However, it is easily observed that this interface-induced band bending is much smaller in InO_x-terminated samples, as the interface related emission has decayed to much less than that of the Al_2O_3/GaAs(100)(6×6) sample. It is to be noted, that in our case the electrons accumulate near the defective sites and escape from the subsurface beneath, which is consistent with the interpretations about lower and higher BE of core-level electrons in these respective areas.

Taking into account the results presented above, we interpret the beneficial effect of indium to be caused by the stabilization of $Ga_xIn_{1-x}As$ crystal surface and subsurface region. The preferential oxygen incorporation into a well-defined crystalline interlayer sheet can prevent the protrusion of O into the subsurface, or the migration of Ga out of the subsurface regions, which would give rise to vacancy-antisite and/or dangling bond defects. The amount of deposited In is an important parameter in the oxygen termination. Well crystallized surfaces can be obtained by employing a wide range of parameters, but not all prevent defect generation as efficiently. Residual Ga oxidation can occur in the case of smallest amount of In, i.e. (1×1), due to the pre-oxidation treatment. As the upward band bending decreases due to In, more charge carriers are present close to the surface, increasing non-radiative recombination through the same As-related defects, which are much more prominent at (1×1) than at the other InO_x structures. Thus the amount of charge carriers in the surface region (due to bending) and the amount of defects do not balance each other out in terms of carrier recombination. An excess of In can also create alternative defects that do not exert such a large band bending effect but that cause alternative charge carrier recombination paths.

4. Conclusion

In summary, it has been reported how a crystalline InO_x interface can be included in an optoelectronic III-V device structure, which resulted in EQE enhancement for the infrared

detector with $Al_2O_3/InO_x/Ga_xIn_{1-x}As$. To understand the beneficial effect of InO_x, we have performed high resolution HAXPES measurements of the Al_2O_3/GaAs junctions with different interfacial InO_x and compared the spectral changes to the PL intensity changes. The results support a defect formation model in which strong Ga oxidation (i.e., Ga_2O_3 formation) causes the rupture of Ga-As bonds, resulting in As dangling bonds that lead to the formation of band-gap states.

Acknowledgements
This work has been supported by University of Turku Graduate School (UTUGS) and the Finnish Funding Agency for Technology and Innovation (TEKES) project COMNINT as well as Academy of Finland (#296469). We thank HZB for the allocation of synchrotron radiation beamtime. R.F is grateful to the Impuls- und Vernetzungsfonds of the Helmholtz Association (VH-NG-423). S.G. thankfully acknowledges the financial support by HZB. The research leading to these results has received funding from the European Community's Seventh Framework Programme (FP7/2007-2013) under grant agreement n.°312284.

Received: ((will be filled in by the editorial staff))
Revised: ((will be filled in by the editorial staff))
Published online: ((will be filled in by the editorial staff))

References

[1] R. S. Smith, I. G. Eddison, *Adv. Mater.* **1992**, *4*,786.

[2] A. Rogalski, *Prog. Quant. Electron.* **2003**, *27*, 59.

[3] C.-S. Lee, C.-T. Hung, B.-Y. Chou, W.-C. Hsu, H.-Y. Liu, C.-S. Ho, Y.-N. Lai, *Semicond. Sci. Tech.* **2012**, *27*, 065006.

[4] K.-W. Lee, W.-S. Chen, *ECS Solid State Lett.* **2013**, *2*, Q9.

[5] Q. Li, X. Zhou, C. W. Tang, K. M. Lau, *IEEE Trans. Electron Dev.* **2013**, *60*, 4112.

[6] J. Yang, M. Shi, X. Shao, T. Li, X. Li, N. Tang, H. Gong, R. Liu, H. Tang, Z.-J. Qiu, *Infrared Phys. Techn.* **2015**, *71*, 272.

[7] S. Yoshida, D. Lin, A. Vais, A. Alian, J. Franco, S. E. Kazzi, Y. Mols, Y. Miyanami, M. Nakazawa, N. Collaert, H. Watanabe, A. Thean, *Appl. Phys. Lett.* **2016**, *109*, 172101.

[8] G. Ariyawansa, C. J. Reyner, J. M. Duran, J. D. Reding, J. E. Scheihing, E. H. Steenbergen, *Appl. Phys. Lett.* **2016**, *109*, 021112.

[9] F. Wang, S. Yip, G. Dong, F. Xiu, L. Song, Z. Yang, D. Li, T. F. Hung, N. Han, and J. C. Ho, *Adv. Mater. Int.* **2017**, *4*, 1700260.

[10] A. C. Seabaugh, Q. Zhang, *Proc. IEEE* **2010**, *98*, 2095.

[11] J. A. Del Alamo, *Nature* **2011**, *479*, 317.

[12] A. Alian, Y. Mols, C. C. M. Bordallo, D. Verreck, A. Verhulst, A. Vandooren, R. Rooyackers, P. G. D. Agopian, J. A. Martino, A. Thean, D. Lin, D. Mocuta, N. Collaert, *Appl. Phys. Lett.* **2016**, *109*, 243502

[13] P. D. Ye, G. D. Wilk, B. Yang, J. Kwo, S. N. G. Chu, S. Naka hara, H.-J. L. Gossmann, J. P. Mannaerts, M. Hong, K. K. Ng, J. Bude, *Appl. Phys. Lett.* **2003**, *83*, 180

[14] M. J. Hale, S. I. Yi, J. Z. Sexton, A. C. Kummel, M. Passlack, *J. Chem. Phys* **2003**, *119*, 6719.

[15] B. Brennan, G. Hughes, *J. Appl. Phys.* **2010**, *108*, 053516

[16] L. Lin, J. Robertson, *J. Vac. Sci. Technol. B* **2012**, *30*, 04E101.

[17] J. Wu, E. Lind, R. Timm, M. Hjort, A. Mikkelsen, L.-E. Wernersson, *Appl. Phys. Lett.* **2012**, *100*, 132905.

[18] M. L. Huang, Y. H. Chang, T. D. Lin, H. Y. Lin, Y. T. Liu, T. W. Pi, M. Hong, J. Kwo, *Appl. Phys. Lett.* **2012**, *101*, 212101.

[19] M. P. J. Punkkinen, P. Laukkanen, J. Lång, M. Kuzmin, M. Tuominen, V. Tuominen, J. Dahl, M. Pessa, M. Guina, K. Kokko, J. Sadowski, B. Johansson, I. J. Väyrynen, L. Vitos, *Phys. Rev. B* **2011**, *83*, 195329.

[20] M. Scarrozza, G. Pourtois, M. Houssa, M. Heyns, A. Stesmans, *Phys. Rev. B* **2012**, *85*, 195307.

[21] J. Dahl, V. Polojärvi, J. Salmi, P. Laukkanen, M. Guina, *Appl. Phys. Lett.* **2011**, *99*, 102105.

[22] C. L. Hinkle, M. Milojevic, B. Brennan, A. M. Sonnet, F. Aguirre-Tostado, G. J. Hughes, E. M. Vogel, R. M. Wallace, *Appl. Phys. Lett.* **2009**, *94*, 162101.

[23] M. Tuominen, M. Yasir, J. Lång, J. Dahl, M. Kuzmin, J. Mäkelä, M. Punkkinen, P. Laukkanen, K. Kokko, K. Schulte, R. Punkkinen, V.-M. Korpijärvi, V. Polojärvi, M. Guina, *Phys. Chem. Chem. Phys.* **2015**, *17*, 7060.

[24] D. Colleoni, G. Miceli, A. Pasquarello, *Phys. Rev. B* **2015**, *92*, 125304.

[25] X. Li, N. Li, X. Zheng, S. Demiguel, J. C. Campbell, D. A. Tulchinsky, K. J. Williams, *IEEE Photonic Tech. Lett.* **2003**, *15*, 1276.

[26] A. Ohtake, *Surf. Sci. Rep.* **2008**, *63*, 295.

[27] M. Gorgoi, S. Svensson, F. Schäfers, G. Öhrwall, M. Mertin, P. Bressler, O. Karis, H. Siegbahn, A. Sandell, H. Rensmo, W. Doherty, C. Jung, W. Braun, W. Eberhardt, *Nucl. Instrum. Meth. A* **2009**, *601*, 48.

[28] F. Schaefers, M. Mertin, M. Gorgoi, *Rev. Sci. Instrum.* **2007**, *78*, 123102.

[29] N. Fairley, *Casa Software Ltd.*, http://www.casaxps.com, accessed: 05, 2017

[30] G. Le Lay, D. Mao, A. Kahn, Y. Hwu, G. Margaritondo, *Phys. Rev. B* **1991**, *43*, 14301.

[31] J. F. Moulder, W. F. Stickle, P. E. Sobol, K. D. Bomben, *Handbook of X-ray photoelectron spectroscopy*, *Vol. 40,* Perkin Elmer Eden Prairie, MN, USA **1992**.

[32] V. Polojärvi, J. Salmi, A. Schramm, A. Tukiainen, M. Guina, J. Pakarinen, E. Arola, J. Lång, I. J. Väyrynen, P. Laukkanen, *Appl. Phys. Lett.* **2010**, *97*, 111109.

[33] D. Colleoni, G. Miceli, A. Pasquarello, *J. Phys. Cond. Mat.* **2014**, *26*, 492202.

[34] D. Colleoni, A. Pasquarello, *Appl. Phys. Lett.* **2015**, *107*, 031605.

[35] D. Colleoni, A. Pasquarello, *Microelectron. Eng.* **2013**, *109*, 50.

[36] C. L. Hinkle, E. M. Vogel, P. D. Ye, R. M. Wallace, *Curr. Opin. Solid State Mater. Sci.* **2011**, *15*, 188.

[37] J. Mäkelä, M. Tuominen, M. Yasir, M. Kuzmin, J. Dahl, M. Punkkinen, P. Laukkanen, K. Kokko, *Appl. Surf. Sci.* **2016**, *369*, 520.

[38] J. J. K. Lång, M. P. J. Punkkinen, M. Tuominen, H.-P. Hedman, M. Vähä-Heikkilä, V. Polojärvi, J. Salmi, V.-M. Korpijärvi, K. Schulte, M. Kuzmin, R. Punkkinen, P. Laukkanen, M. Guina, K. Kokko, *Phys. Rev. B* **2014**, *90*, 045312.

[39] L. A. Walsh, G. Hughes, J. Lin, P. K. Hurley, T. P. O'Regan, E. Cockayne, J. C. Woicik, *Phys. Rev. B* **2013**, *88*, 045322.

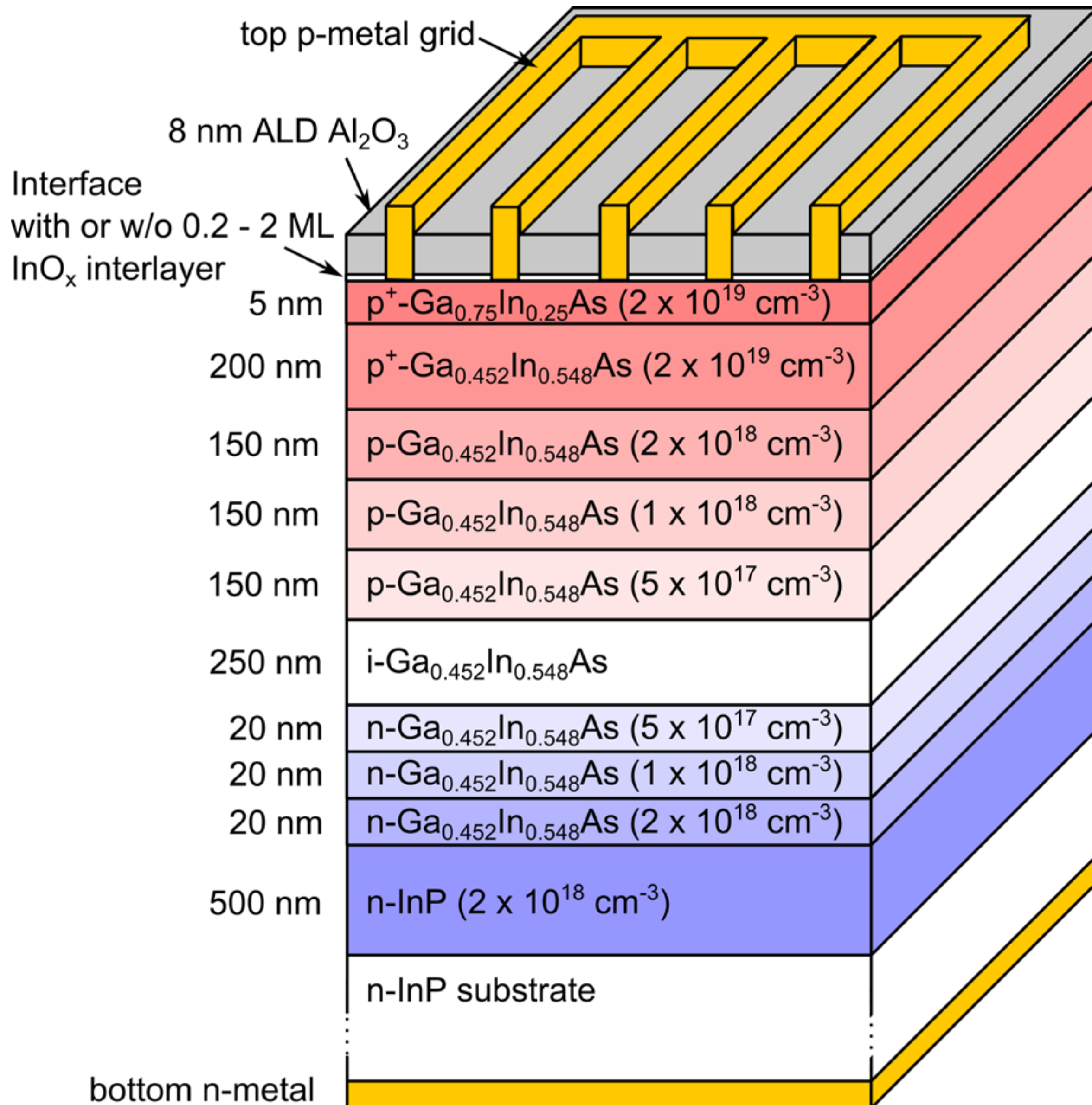

Figure 1. Cross-sectional schematic view of the IR detector. Thicknesses are shown next to the corresponding layer and doping concentrations in parentheses. Figure is not to scale.

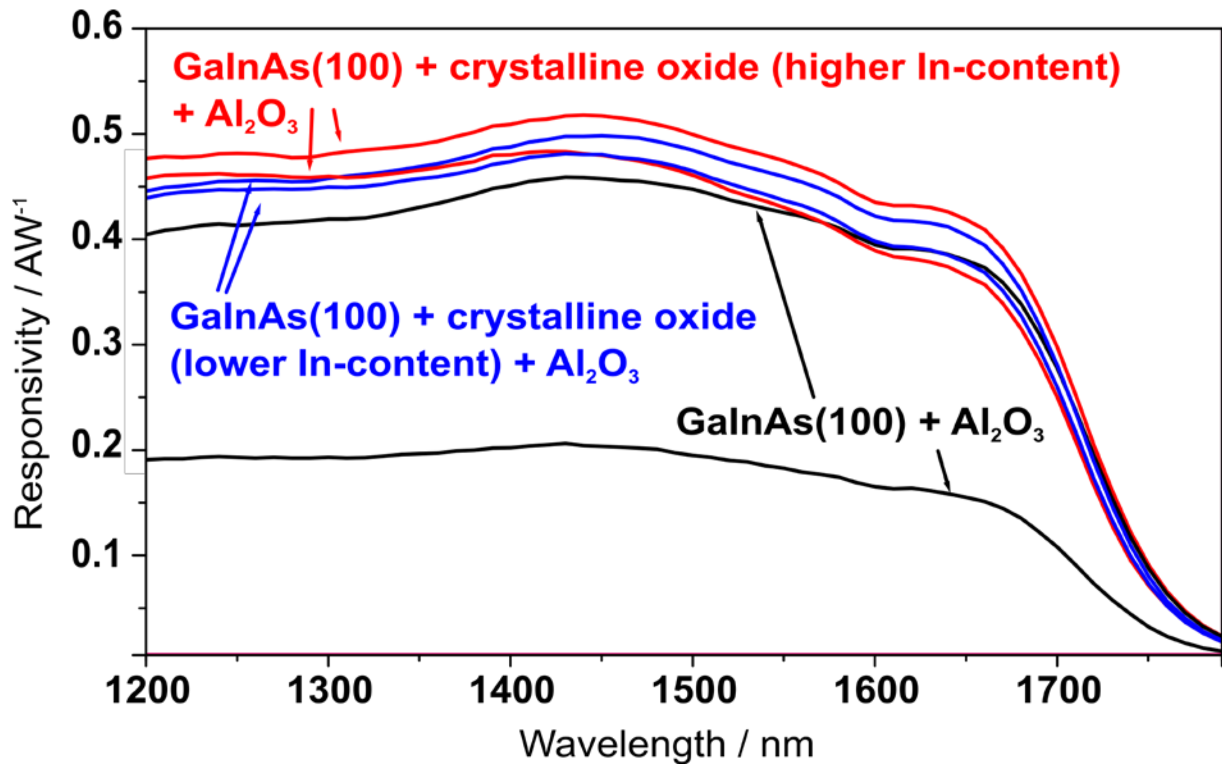

Figure 2. Responsivity data measured from GaInAs photodetectors with and without crystalline oxide InO_x interlayer. Reducing evaporated In-content on the surface from calibrated $c(4\times2)$ parameters results in decreased responsivity.

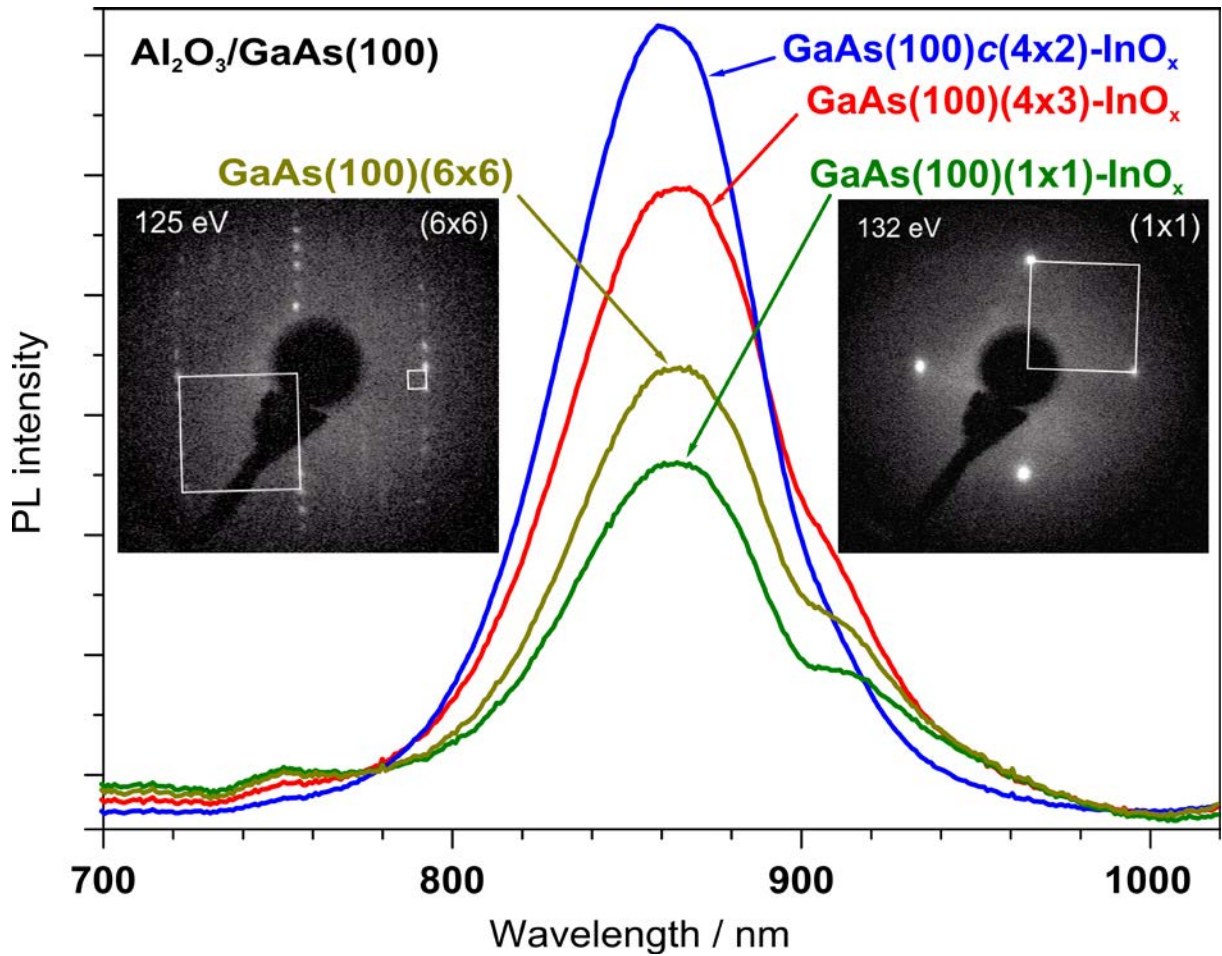

Figure 3. PL (excitation: 14 J, 532 nm at RT) and LEED data measured from the GaAs(100) samples. Al_2O_3/GaAs(100)*c*(4×2)-InO_x exhibits the highest PL intensity, i.e. lowest density of defects.

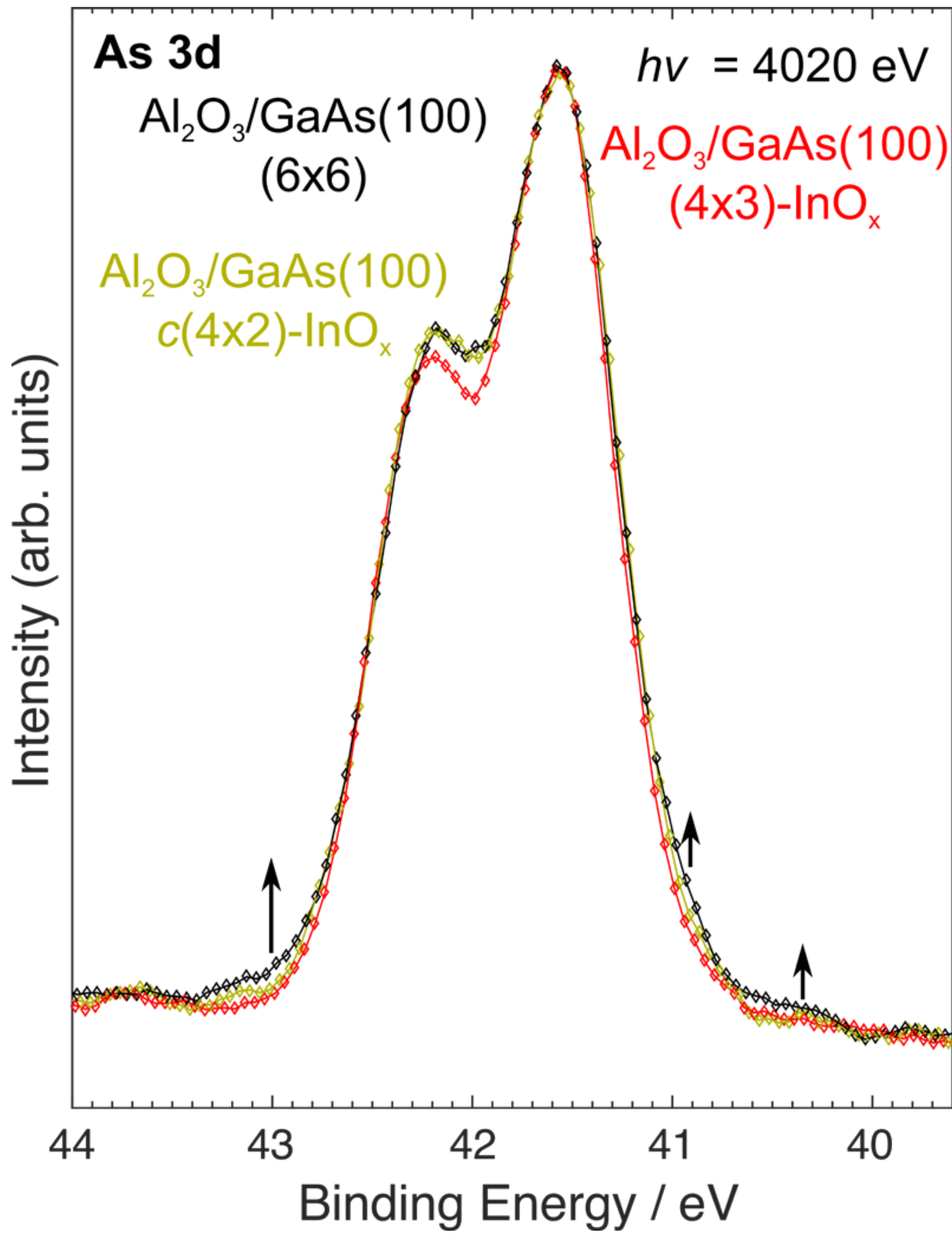

Figure 4. As 3d spectra of the Al_2O_3/GaAs(100)(6×6), *c*(4×2)-InO_x and (4×3)-InO_x samples showing distinct differences in peak intensities adjacent to the intensity maxima. Separated features are shown with arrows that are scaled to show the rough difference from the other spectrum. Peaks are calibrated to have same binding energy at maximum intensity to emphasize differences in peak shapes.

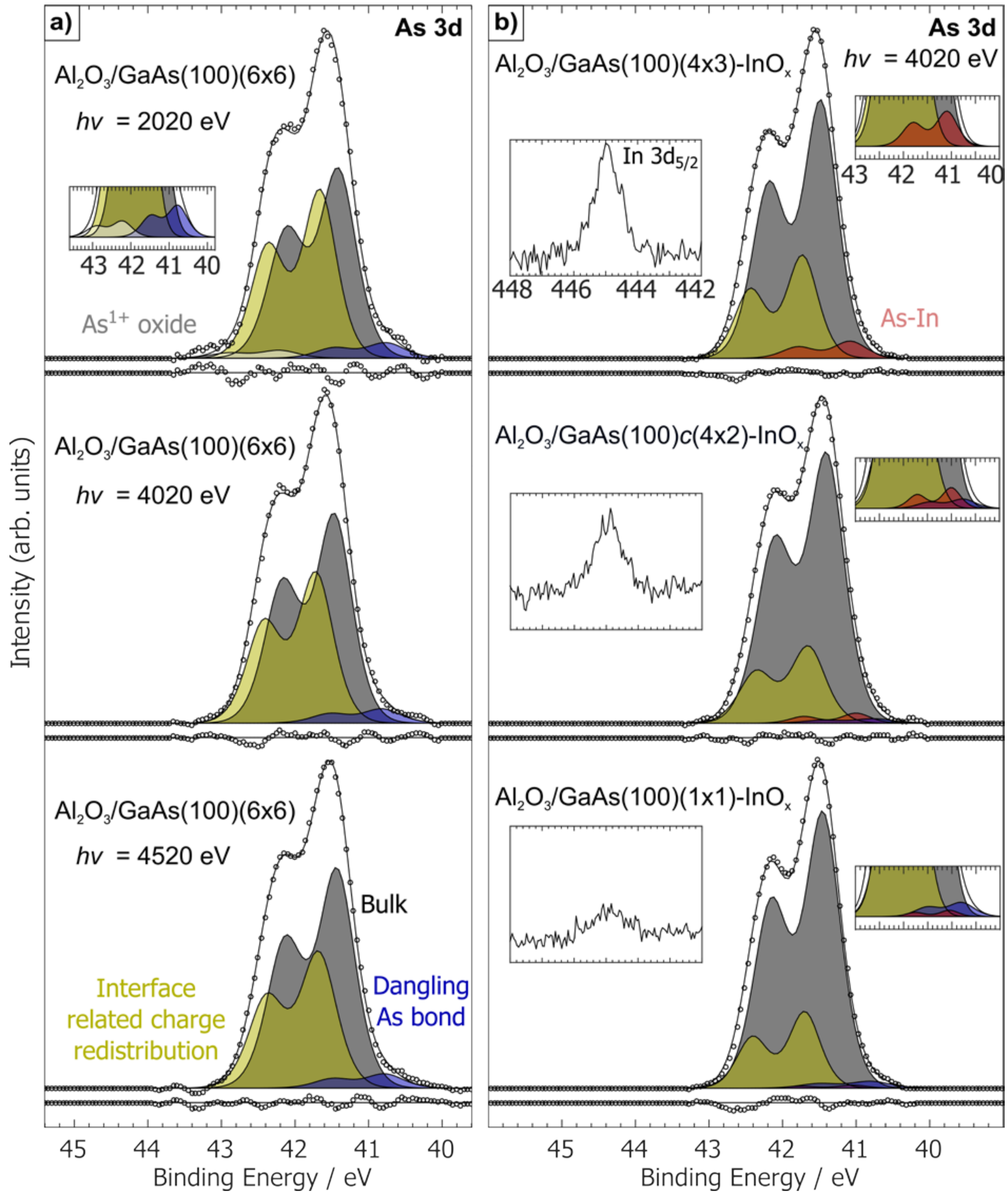

Figure 5. Curve fitted As 3d spectra of the a) Al_2O_3/GaAs(100)(6×6) sample with different photon energies for depth profiling, and b) with *hv* = 4020 eV of crystalline oxidized Al_2O_3/GaAs(100) samples with different InO_x-reconstructions. Fitting residual is plotted in scale beneath each spectrum.

Novel crystalline oxide structure between GaAs(100) and ALD grown Al_2O_3 is shown to result in improvement of practical IR detectors. Hard x-ray photoelectron spectroscopy analysis shows that different InO_x structures can give rise to different charge carrier recombination mechanisms, but they are straightforwardly suppressed with an optimal amount of In in the interfacial layer.

GaAs, oxide, interface, defects, HAXPES

J. Mäkelä, M. Tuominen, J. Dahl, S. Granroth, M. Yasir, J.-P. Lehtiö, R.-R. Uusitalo, M. Kuzmin, M.P.J. Punkkinen, P. Laukkanen*, K. Kokko, R. Félix, M. Lastusaari, V. Polojärvi, J. Lyytikäinen, A. Tukiainen, M. Guina

Decreasing Defect-state Density of Al2O3/GaxIn1-xAs Device Interfaces with InOx Structures